

A Look at the Optimization of Robot Welding Speed Based on Process Modeling

Integrating robot simulation, finite element analysis, and numerical optimization provides a powerful tool for constructing and optimizing off-line robot torch trajectories and process parameters

BY M. ERICSSON AND P. NYLÉN

ABSTRACT. Simulation tools to search for optimal process parameters are of great interest to reduce the number of experiments and thereby reduce cost and production time. In this paper, robot simulation has been used in combination with finite element simulations to optimize robot speed in order to minimize distortion while keeping complete joint penetration. In an earlier work performed by the authors, a finite element model was developed to predict heat transfer and residual stresses of parts with complex shapes. An interface between a robot simulation model and a finite element analysis model was also constructed. In this paper, an iterative method for robot speed optimization has been developed using MATLAB. The algorithm is designed to maintain complete joint penetration while maximizing productivity by utilizing the fastest weld speed. The method makes it possible to optimize the heat input to the component and thereby minimize component deformation for parts with complex shapes.

The system was evaluated on stainless steel plates with varying thicknesses. Robot weld paths were defined off line and automatically downloaded to the finite element software where the optimization was performed. Simulations and experimental validations are presented.

Introduction

CAD-based path planning of robot-welded parts is an elegant technique. Using this method, the programming is moved away from the robot to a graphical computer system often referred to as an off-line programming (OLP) system. This method makes it possible to maintain constant velocity, distance from, and orientation with respect to a part with complex shape. This would be virtually impossible using manual programming. The OLP

technology is well established in industry and has been an active research area (Refs. 1–4) for some ten years. There is, however, a need for a computer-aided process planning tool by which process parameters could be defined and optimized off line. This functionality does not exist in commercially available OLP tools today. Such a system should be capable of optimizing process parameters such as welding speed and power due to variations in part geometry (thickness variation), material, and part temperatures (heat sources). Of specific interest is to determine an optimal weld speed, i.e., the speed that generates the lowest component deformation while keeping complete joint penetration. Such a process-planning tool could be developed by a combination of robot simulation and finite element simulations. Finite element analysis (FEA) for welding process simulations on fairly simply shaped parts is a well-established technique (Refs. 5–11). It is usually used to investigate structural behavior, usually to predict residual stresses. Manufacturing simulations to plan welding sequences and to optimize process parameters or fixture designs are still rare, specifically simulations of complex three-dimensional parts.

In earlier works performed by the authors, integration between a robot simulation model and a FEA model was proposed (Refs. 12–14). This model was developed to predict heat transfer residual stresses and fixture forces considering parts with complex shapes. In the present study work, a MATLAB implementation of an iterative method to optimize weld

speed and thereby minimize component deformation is described. Simulations and optimizations on plates with varying thickness are presented. A validation of the temperature predictions is performed by comparing the predictions with thermocouple- and IR-measured temperatures. A brief description of the OLP-FEA integration as well as the process model are also summarized. A more detailed description of these models can be found in Refs. 12–14.

Principle of Off-Line Programming (OLP) and Integration with the FEA Model

The overall architecture of the simulation system is given in Fig. 1. The programming of the robot motion is based on a simulation of the process by the IGRIP system of Deneb, Inc. The model consists of two main parts: a) a geometric, kinematic, and dynamic model of the robot, and b) a model of the workpiece to be welded. The workpiece model is usually first constructed in a CAD/CAM system and afterward exported to the OLP system. The geometrical as well as the kinematic model of the work cell are usually made directly in the OLP system. In this system, a weld trajectory is also generated by defining torch locations and orientations. This trajectory is then simulated, and checks for collisions between the workpiece and the weld gun are made. Checks for and elimination of robot singularities are also made. A calibration of the model with the real cell is thereafter done; this can include several sub steps such as tool point, workpiece, and signature calibration (Ref. 1). A translation of the program to a specific robot manufacturer language is made, and the robot coordinates, welding speeds, and process parameters are finally exported from the OLP model to the FEA model where a heat and residual stress prediction is made. The principle of this FEA model is given in the next section.

KEYWORDS

Robot Simulation
Off-Line Programming (OLP)
Welding Speed
Finite Element Analysis (FEA)
Temperature
Weld Velocity

M. ERICSSON (Mikael.Ericsson@hv.se) and P. NYLÉN are with University West, Sweden.

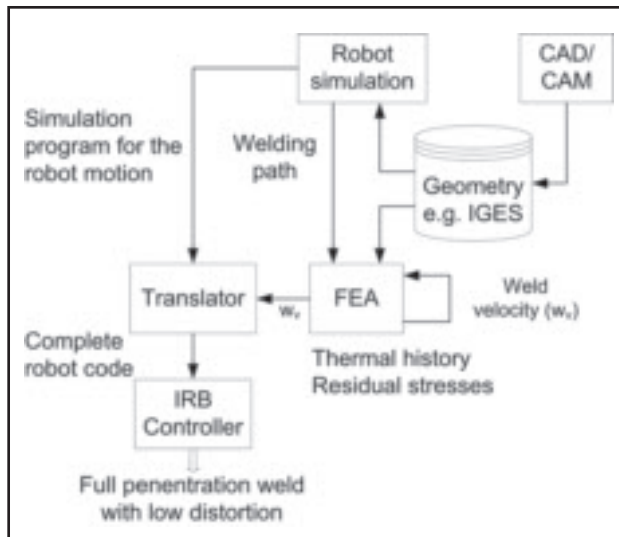


Fig. 1 — The overall architecture of the simulation system.

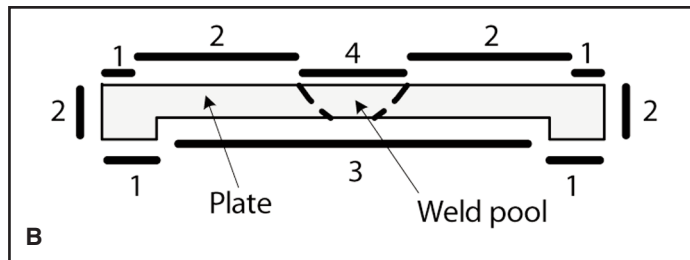
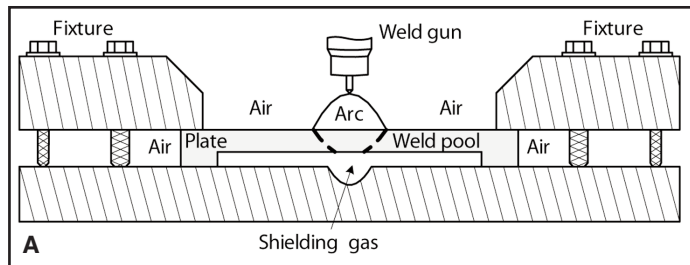


Fig. 2 — Principle outline of applied boundary conditions in the FEA model.

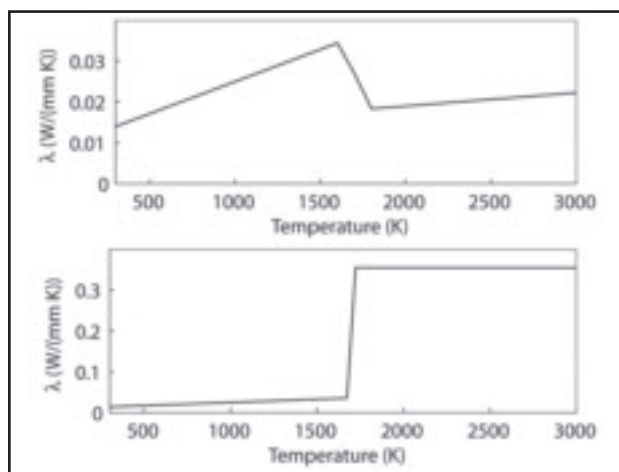


Fig. 3 — Conductivity for SS 316L. Top — Original values (Ref. 20); bottom — increased with a factor 10 above the liquidus temperature.

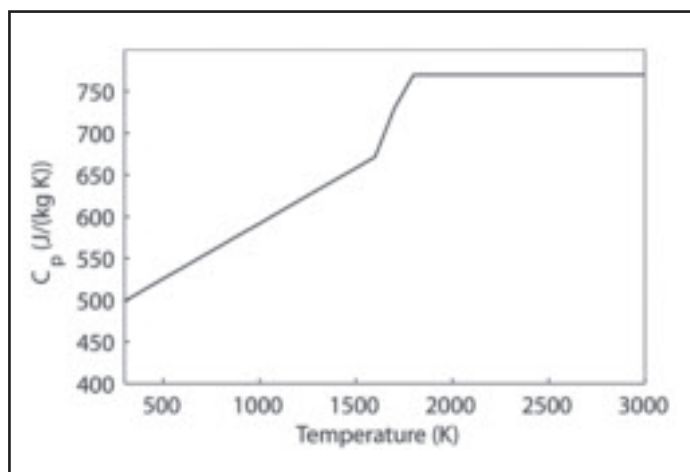


Fig. 4 — Specific heat for SS 316L (Ref. 20).

The Heat Transfer Model

A finite element analysis model was used to predict the temperature evolution outside the molten zone. The FEA program Marc from MSC Software was used. User subroutines were developed in earlier work to simulate a moving heat source (Refs. 12–14). A Gaussian surface distribution was used. This distribution was preferred to a volumetric one (Ref. 8) because it reduces the number of parameters (unknown variables) to be fit. The surface heat flux distribution was expressed as (Ref. 11)

$$q = q_0 \cdot e^{-\alpha_q r^2}$$

$$q_0 = \frac{\eta EI \alpha_q}{\pi} \quad (1)$$

where q denotes the heat transferred to the workpiece, E the voltage, I the current, η the efficiency factor, α_q the concentration factor, and r the radial distance from the center of the heat source. This distribution was truncated in the radial direction, at a cut-off limit of 5% of the maximal heat input, as proposed by D. Radaj (Ref. 11). The parameter α_q in the heat flux distribution was set to achieve a fusion zone fitting experimental data obtained by measuring the top side and root side widths of cross sections of welds. Experimental trials were made on plane plates to find an appropriate value of the dimensionless parameter α_q . A value of 0.1 was selected, which gave good agreement between predicted geometry of the fusion zone and corresponding measured zone. This parameter fit was considered necessary because a semi-empirical approach such as

proposed by Ref. 15 was not possible due to the short electrode distance (1.5 mm), which made photographing of the welding

Table 1 — SS 316L Physical Properties (Refs. 19–21)

Nomenclature	Symbol	Value	Unit
Density	ρ	$7.3 \cdot 10^{-6}$	kg/mm ³
Latent heat of fusion	D_H	$2.47 \cdot 10^{-5}$	J/kg
Solidus temperature	T_{sol}	1673	K
Liquidus temperature	T_{liq}	1723	K
Thermal conductivity	k	see Fig. 3	
Heat capacity Initial temperature	C_p T_0	see Fig. 4 293	K

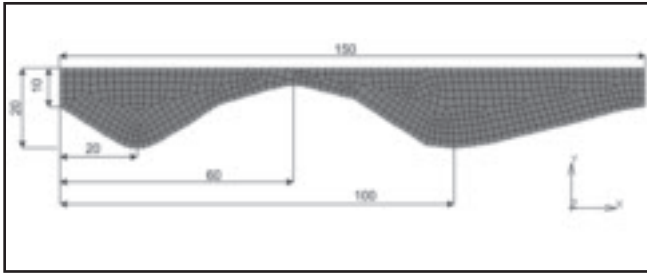


Fig. 5 — Cross section and computational mesh of two-dimensional part. Dimensions in mm.

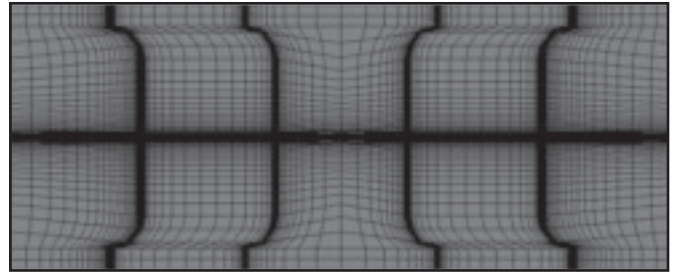


Fig. 6 — Cross section and computational mesh of the three-dimensional part. Note the high mesh density along the weld path and close to the steps.



Fig. 7 — Profile of the three-dimensional part. A — Along the weld path; B — perpendicular to the weld path. All dimensions in mm.

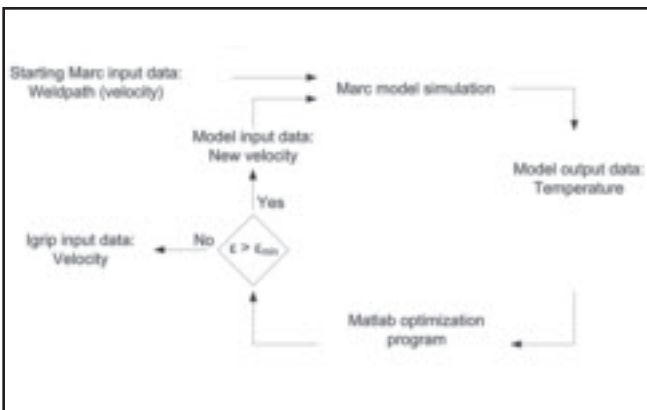


Fig. 8 — Principle of optimization. Loop until $\epsilon > \epsilon_{min}$.

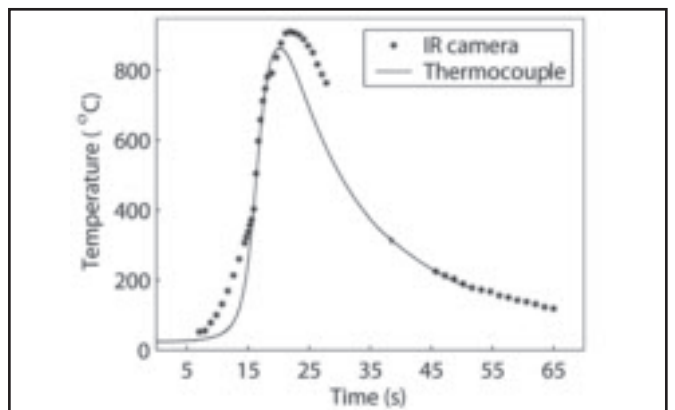


Fig. 9 — Thermocouple- and IR-measured temperatures.

arc not possible. The efficiency factor η was estimated experimentally using the method proposed by Ref. 16. The electrode was kept still at a distance 1.5 mm from the plate. A very high efficiency was determined, $\eta = 0.90$; the value higher than other proposed efficiency values, 0.6 to 0.85 (Refs. 17, 18). The major reason

for this high value might be the short electrode distance used. Both α_q and η were kept constant through all simulations. This assumption was considered justifiable because the electrode distance and current were kept constant. Convection boundary conditions were applied to the free surface dissipating energy as well as at

the contact surfaces between fixture and plates. Figure 2 shows the applied boundary conditions. A flow of argon (Table 1), was used to protect the root side of the weld. The heat transfer coefficients were set to $2 \cdot 10^{-5} \text{ W/m}^2$ at the topside of the plate (number 2 in Fig. 2B), and to $2 \cdot 10^{-4} \text{ W/m}^2$ at the root side of the weld (number

Table 2 — Process Parameters Used

Parameter	Value
Current	100 A
Voltage	10 V
Weld velocity	Optimized mm/s
Root gas flow rate (argon)	20 L/min
Shielding gas (argon)	17 L/min
Arc length	1.5 mm
Filler metal	none

Table 3 — Measured and Predicted Fusion Zones

Location (see Fig. 17)	Welding Speed (mm/s) (see Fig. 16)	Measured W_t (mm)	Measured W_r (mm)	Predicted W_t (mm)	Predicted W_r (mm)
A	13.8	3.29	0.76	3.71	1.67
B	4.5	4.79	1.47	5.24	2.44
C	2.1	6.15	1.0	7.1	2.24
D	4.7	5.16	1.12	5.24	1.26
E	14.0	4.09	3.25	3.11	0.51

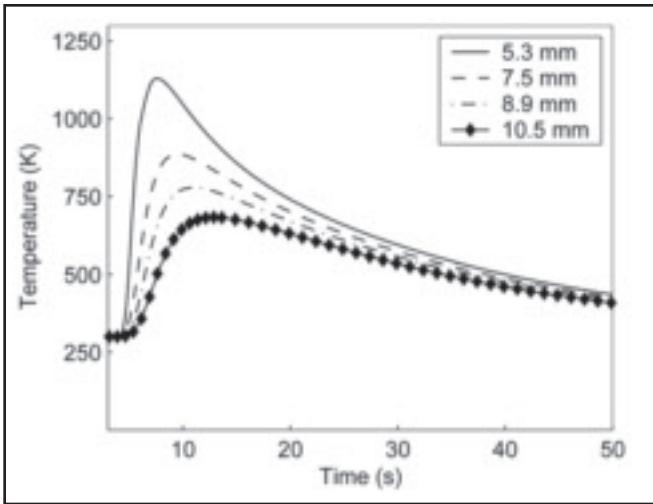


Fig. 10 — Predicted temperature-time histories.

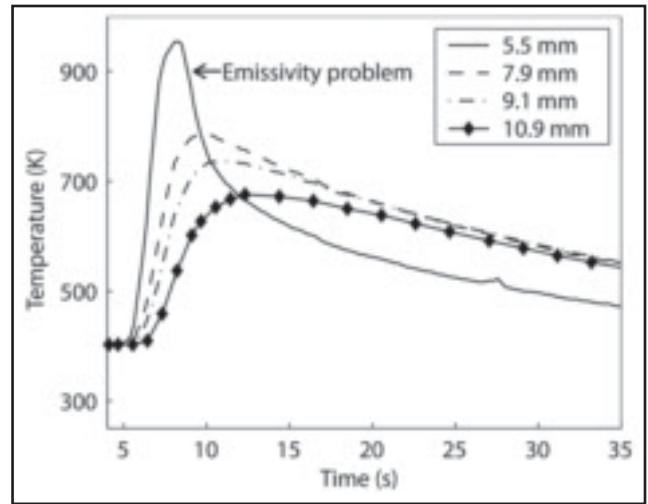


Fig. 11 — Measured temperature-time histories.

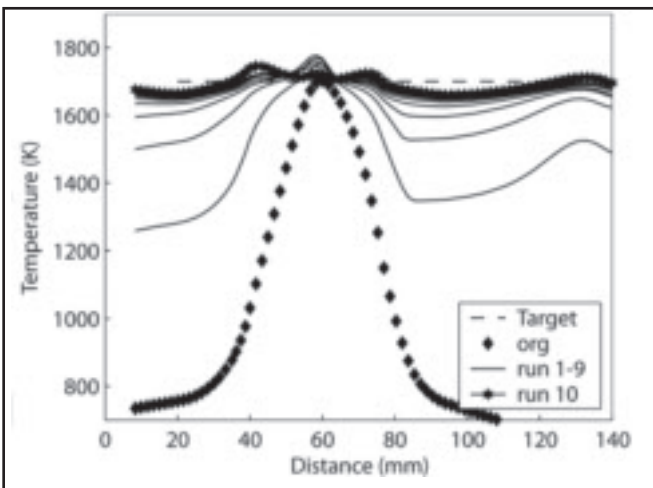


Fig. 12 — Predicted temperatures at the root side in the center of the weld. The target temperature is 1700 K.

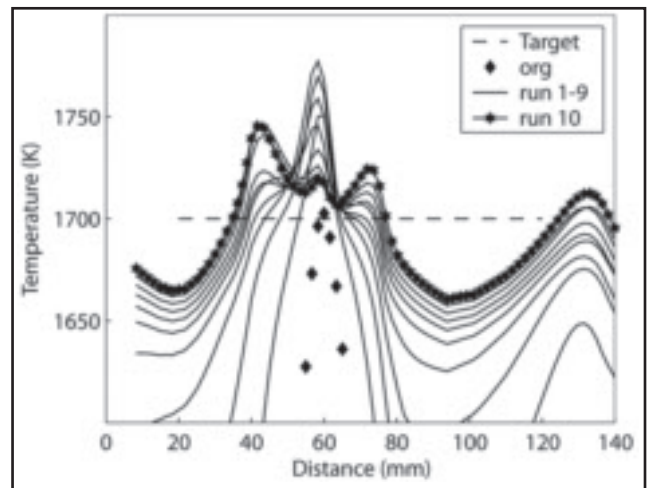


Fig. 13 — Close up of predicted temperatures around 1700 K at the root side at the center of the weld.

3 in Fig. 2B), because forced cooling by argon was applied at the root side of the plates. The contact surfaces between the plates and the fixtures were assumed to have a heat transfer coefficient of 10^{-3} W/m² (number 1 in Fig. 2B). The location of the arc is indicated with number 4 in Fig. 2B.

The material properties used are given in Table 1.

Temperature-dependent properties such as thermal conductivity and specific heat were used — Figs. 3, 4. Phase change was included in the analysis. Weld pool convection has been shown to strongly affect the heat transfer in the weld pool. This convection, however, has to be artificially treated in a solid mechanical model by multiplying the thermal conductivity by a

certain factor when the temperature exceeds the liquidus temperature. This method has been commonly used (Refs. 22–24). An intensive circulation was noted and a factor of 10 was selected. The same factor has also been used in earlier work (Refs. 12–14) — Fig. 3.

The computational domain was discretized by a nonuniform mesh with higher densities in regions close to the weld path as well as where steep thickness variations were present. Eight-node brick elements were used — Figs. 5, 6.

To verify the proposed optimization method, two different geometries were defined: a) a two dimensional plate (referred to as part A) with continuously varying thickness according to Fig. 5, and b) a three-dimensional plate (referred to

as part B) with stepwise varying thickness — Figs. 6, 7. Grid sensitivity trials were made for part B. The final mesh for this part consisted of 144,000 elements. A constant time step of 0.05 s was used.

Robot Speed Optimization

Once the robot path and the desired root side temperature are chosen, the robot speed can be optimized. The liquidus temperature was a natural choice for input for the optimization because the main purpose was to control penetration. The following algorithm was used, starting from a given robot speed s_0 along the trajectory:

- 1) Compute the maximum temperature T_{Max_i} along the trajectory by simulat-

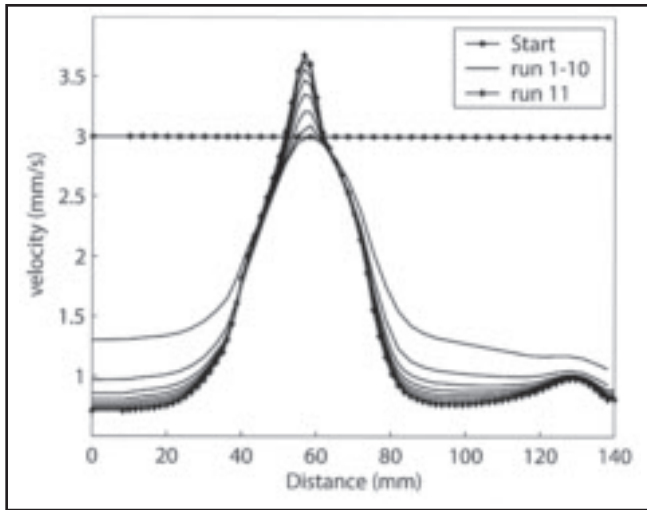


Fig. 14 — Calculated weld velocities for the first 11 iterations. The velocity was set to 3 mm/s in the first iteration.

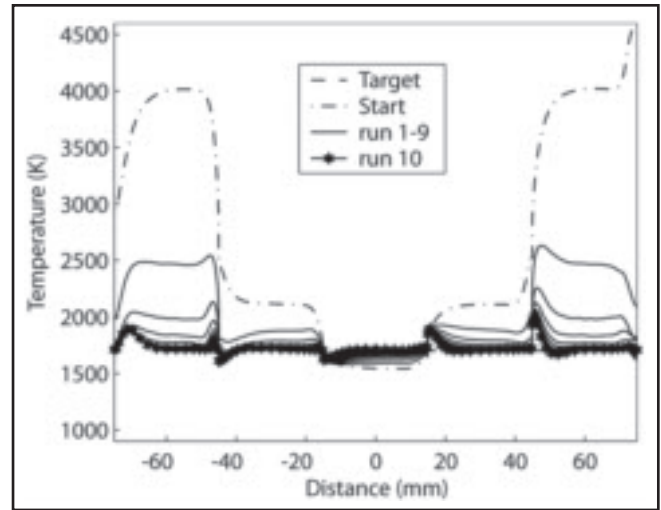


Fig. 15 — Predicted temperatures at the root side in the center of the weld. The target temperature is 1700K.

ing the weld using the speed s_i

2) Update the speed along the trajectory using the iteration

$$s_{i+1} = s_i \left(1 + \lambda \frac{T_{max_i} - T_{melt}}{T_{melt}} \right) \quad (2)$$

Here λ is a relaxation parameter, T_{melt} the liquidus temperature, and T_{max} the maximum temperature at each node. The iteration corresponds to increasing the robot speed when the temperature becomes too high. As the computational cost of one iteration is very low compared to the temperature calculation, each iteration is cheap. It should, however, be noticed that the proposed method is not an optimization method in the usual sense since it does not always converge to a local or global optimum. Iterations are therefore performed until the error (ϵ) no longer decreases. The principle of the overall optimization is given in Fig. 8. An initial robot speed is defined in IGRIP and downloaded to Marc where the temperature calculation is performed. The root side temperatures are compared with the liquidus temperature and a new robot speed vector is calculated. The calculations continue iteratively until an optimal velocity vector is found, i.e., the velocity vector that maximizes the speed while keeping complete joint penetration. This velocity vector is finally exported back to IGRIP for final process simulation.

Experiments

Gas tungsten arc welding (GTAW) was performed on plane plates in order to validate the temperature predictions and to be able to determine the concentration

factor (α_q in Equation 1) using an in-house robotized welding cell. The torch used was from Binzel AB and was mounted onto a six-axis IRB1400 robot from ABB. The power source was a TIG Commander 400 AC/DC from Migatron AB. Throughout all experiments, thoriated tungsten electrodes were used. The process parameters are shown in Table 2.

Both thermocouples and high-resolution infrared (IR) emission measurements were used for the temperature measurements. Six thermocouples were positioned perpendicularly to the welding direction. The first gauge was positioned as close as possible to the melted zone at a distance of 4 mm from the center of the weld. The rest of the thermocouples were positioned 0.5 mm radially from the first gauge along the radial direction. The sampling frequency was 270 Hz for each thermocouple. The IR camera was a VARIOSCAN high resolution, from JENOPTIK, Laser, Optik, Systeme GmbH, that works in the IR radiation spectrum of 8–12 μm . The camera was used both in a line scan mode with a scanning frequency of 270 Hz, as well as in a full-frame mode with a frequency of 1 Hz. The analysis of the IR measurements was made using the IRBIS Plus software provided by JENOPTIK. A

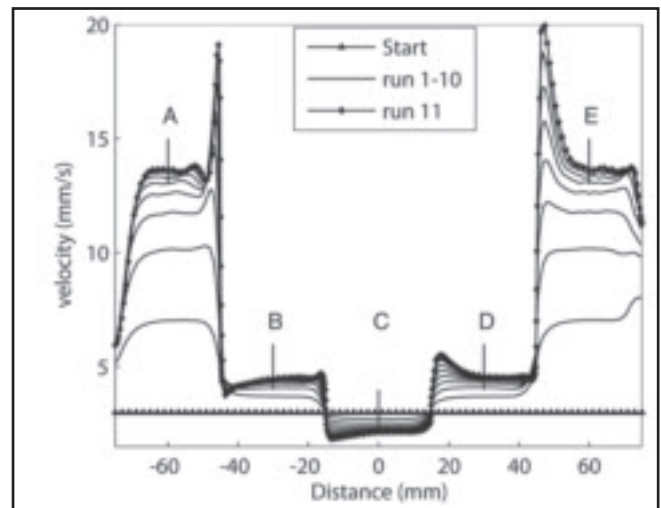


Fig. 16 — Calculated weld velocities for the first ten iterations. The velocity was set to 3 mm/s in the first iteration.

comparison between the IR results with the thermocouple was made. The plates were sooted before welding in order to reduce the emissivity dependency in the IR measurements. A more detailed description of the sooting technique and the IR measurement principle can be found in Ref. 25.

Results and Discussion

The thermocouple- and IR-measured temperature histories in a point located 7mm from the center of the weld are given in Fig. 9.

There is good agreement between the two techniques. The predicted and corresponding IR-measured temperatures at location B, see Fig. 17, are given in Figs. 10 and 11, respectively. Due to soot evap-

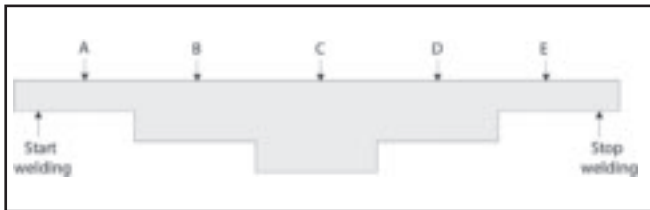


Fig. 17 — Cutting position on part B.



Fig. 18 — Welded cross section.



Fig. 19 — Predicted cross section.

oration close to the weld seam, reliable temperature measurements could not be made at 5.5 mm — Fig. 11. The conclusion from this comparison was that the model was capable of predicting the thermal cycle well.

The predicted temperatures and weld velocities for the first ten iterations for part A are given in Figs. 12 and 14, respectively. Figure 13 shows the temperature close to the target temperature. The temperatures correspond to values predicted along the root side symmetry curve, i.e., the weld centerline. The target temperature for the simulation was set to 1700 K, which corresponds to a complete joint penetration weld. The optimization algorithm converges quickly. After five iterations, the temperature discrepancy had already reached ± 100 K, and after ten iterations this discrepancy went down to ± 30 K. The weld velocity was initially set to 3 mm/s and it varied between 0.7 to above 3.5 mm/s after ten iterations. The maximum difference in velocity between iteration 10 and 11 is 0.0167 mm/s. Further optimization was not of interest because this velocity compares with the robot accuracy.

The predicted temperatures and weld velocities for the first ten iterations for part B are given in Figs. 15 and 16, respectively. The temperatures correspond to values predicted 0.1 mm radial to the weld center-line at the root side. This offset was selected to guarantee complete joint penetration. Also, in this case, the target temperature was set to 1700 K. The temperatures calculated at the first iteration are unrealistically high, but soon approach the target temperature. The convergence is slower in this case than for case A. A temperature peak of about 2010 K

still exists in the tenth iteration. This peak is due to the step change in thickness. The weld velocity also shows a more dramatic variation for this plate, with values in the range 2–20 mm/s. The weld velocity was initially set to 3.0 mm/s. The average difference in velocity between iteration 10 and 11 is 0.0815 mm/s.

It was not considered of interest to optimize the velocity further, i.e., to try to eliminate the peaks in Figs. 15 and 16 because the case was selected mainly to demonstrate the technique. The step change in thickness would in practice demand a change in size of the melt pool. Part B was welded using the parameters given in Table 2. Figure 17 shows the IR measuring position (B) and locations where cross sections were evaluated. There was a fairly good agreement between measured and predicted fusion, (Table 3). Predicted values are in general somewhat larger except for location E. This might be due to the location of E close to the end point of the weld joint. Another possible explanation for this discrepancy was distortion, which increased the electrode distance.

Figure 18 shows a welded cross section of part B at location D — Fig. 17. Corresponding cross section from the simulation is given in Fig. 19.

The overall conclusion from the optimization was that although simple, the proposed optimization algorithm performed very well. Several extensions of this method are possible. It would be of interest to include residual stresses or deformation, for instance. Different welding sequences could also be automatically evaluated. It would also be valuable to extend the process model to include welding wire and pulsed current.

Conclusions

A simple yet effective method has been successfully developed and implemented to optimize the welding speed. The proposed method allows optimizing the heat input to the component and thereby minimize component deformation for parts with complex shapes. The process model was initially validated comparing temperature predictions with experimental measurements, and a good agreement was found. The optimization algorithm was evaluated for two different test cases, a two-dimensional plate with continuously varying thickness and a three-dimensional plate with stepwise varying thickness. The temperature converged quickly for the two-dimensional case and reached a variation of ± 30 K around the target temperature within ten iterations. For the second test case, a temperature peak of about 2010 K still existed in the tenth iteration due to the discrete variation in thickness. The weld velocity also showed a more dramatic variation for this plate, with values in the 2–20 mm/s range.

The proposed method to integrate robot simulation, finite element analysis, and numerical optimization provides a promising and powerful tool for constructing and optimizing off-line robot torch trajectories and process parameters. The method can also be an efficient tool in early product development to evaluate different design concepts. The proposed optimizing algorithm was shown computationally efficient, putting less demand on computational power, thus making industrial usage possible.

Acknowledgment

The authors wish to acknowledge the assistance in calculations by Benoit Ripaud of University West, the assistance in the laboratory by Kjell Hurtig and Mats Högström of University West, and to Al Henry of University West for linguistic revision. The work was funded by the Foundation for Knowledge and Competence Development.

References

1. Bolmsjö, G., Olsson, M., and Brink, K. 1997. Off-line programming of GMAW robotic

systems — a case study. *Int. J. for the Joining of Materials* 9(3): 86–93.

2. Buchal, R. O., Cheras, D. B., Sassani, F., and Duncan, J. P. 1989. Simulated off-line programming of welding robots. *Int. J. of Robotics Research* 8(3): 31–43.

3. Bolmsjö, G. 1999. Programming robot welding system using advanced simulation tools. *Proc. of the International Conf. on the Joining of Materials JOM-9*, 284–291.

4. Walter, S. 1994. Simulation and calibration for off-line programming of industrial robots. *Proc. of Computer Technology in Welding*, Paper 54.

5. Eagar, T. W., and Tsai, N. S. 1983. Temperature fields produced by traveling distributed heat sources. *Welding Journal* 62(12): 346-s to 355-s.

6. Gu, M., Goldak, J., and Hughes, E. 1993. Steady state thermal analysis of welds with filler metal addition. *Canadian Metallurgical Quarterly* 32(1): 49-s to 55-s.

7. Kou, S., and Le, Y. 1983. Three-dimensional heat flow and solidification during autogenous GTA welding of aluminum plates. *Metallurgical Transactions A* 14A: 2245-s to 2253-s.

8. Goldak, J., McDill, M., Oddy, A., House, R., Chi, M., and Bibby, M. 1987. Computational heat transfer for weld mechanics. *Proc. of Int. Conf. on Trends in Welding Research, Advances in Welding Science and Technology*. Eds. S. A. David: 15–20. Metals Park ASM Int.

9. Jonsson, M., Karlsson, L., and Lindgren, L. E. 1985. Deformation and stresses in butt welding of large plates with special references to the material properties. *J. of Eng. Mat. and*

Tech. 107: 265-s to 270-s.

10. Lindgren, L. E., and Karlsson, L. 1988. Deformation and stresses in welding of shell structures. *Int. J. for Numerical Methods in Eng.* 25: 635-s to 655-s.

11. Radaj, D. 1992. *Heat Effects of Welding*: 33 Berlin: Springer-Verlag.

12. Ericsson, M., Bolmsjo, G., and Nylén, P. Three-dimensional simulation of robot path and heat transfer of a TIG-welded part with complex geometry. SME technical paper AD02-292 (Dearborn, Mich.: Society of Manufacturing Engineers, 2002). 2001, *Proc. 11th International Conference on Computer Technology in Welding*.

13. Ericsson, M., Nylén, P., Berglund, D., and Lin-Peng, R. 2005. Three dimensional simulation of robot path, heat transfer and residual stresses of a welded part with complex geometry. *Int. J. for the Joining of Materials* 17(2).

14. Ericsson, M. Simulation of robotic TIG-welding. Technical licentiate thesis. ISBN 91-628-5702-9 2003-05-15.

15. Connor, L. P., ed. 1991. Welding technology. *Welding Handbook*, Vol 1, 8th Ed. American Welding Society.

16. Bisen, K. B., Arenas, M., El-Kaddah, N., and Acoff, V. L. 2003. Computation and validation of weld pool dimensions and temperature profiles for gamma TiAl. *Metallurgical and Materials Transactions* 34 A: 2273–2279.

17. Connor, L. P., ed. 1991. Welding technology. *Welding Handbook*, Vol. 1, 8th ed. American Welding Society.

18. Goncalves, C. V., Vilarinho, L. O., Scotti, A., and Guimaraes, G. 2006. Estimation of heat

source and thermal efficiency in GTAW process by using inverse techniques. *Journal of Materials Processing Technology* 172: 42–51.

19. Choo, R. T. C., Szekeley, J., and David, S. A. 1992. On the calculation of the free surface temperature of gas tungsten arc weld pools from the first principles — Part II: Modelling the weld pool and comparison with experiments. *Metallurgical Transaction B* 23B: 371–384.

20. Choong, S. K. 1975. Thermophysical properties of stainless steel, ANL-75-55, Argonne, Ill.

21. Toselo, I., Tissot, F. X., and Barras, M. Modelling of the weld behaviour for the control of the GTA process by computer aided welding, Commissariat a l'Energie atomique, Centre d'Etudes et de Recherche sur les Materiaux, Gif sur Yvette.

22. Lindgren, L-E. 2001. Finite element modeling and simulation of welding, Part 2: Improved material modeling. *Journal of Thermal Stresses* 24: 195–231.

23. Goldak, J., and Akhlaghi, M. 2005. *Computational Welding Mechanics*, Springer Science + Business Media, Inc.

24. Michaleris, P., and DeBiccari, A. 1997. Prediction of welding distortion. *Welding Journal* 76(4): 172-s to 181-s.

25. Henrikson, P., and Ericsson, M. 2002. Non-contact temperature measurements using an infrared camera in aerospace welding research. *Proc. 6th International Conference on Trends in Welding Research*, 930–935.

CALL FOR PAPERS AWS Detroit Section International Sheet Metal Welding Conference XIII May 14–16, 2008 Detroit, Michigan

The International Sheet Metal Welding Conference Technical Committee is actively seeking abstracts related to joining technologies for thin sheet fabrications. Typical categories include:

- Resistance Welding Processes
- Friction Joining Processes
- Advanced High-Strength Steels
- Application Studies
- Arc Welding Processes
- Hybrid Joining Processes
- Thin and Lightweight Materials
- Process Modeling
- High-Energy Beam Processes
- Innovative Joining Processes
- Coated Materials
- Process Monitoring and Control

A technical abstract in a format that is compatible with MS Word, along with a completed Author Application Form must be submitted to the Technical Committee Chairman by September 21, 2007. Abstracts to be considered must be of sufficient detail for a fair evaluation of the work to be presented. The paper must be related to sheet metal alloys and/or joining processes used in manufacturing of commercial products. It is not a requirement that your presentation be an original effort. Case histories, reviews, and papers that have been previously published or presented will be considered as long as they are pertinent to the general interests of the conference attendees.

All abstracts will be considered by the Technical Committee. It is expected that the Committee's selections will be announced by November 14, 2007. Authors must submit a manuscript to the Committee by March 19, 2008. The Proceedings will be available to all attendees at the beginning of the Conference.

You may also download additional information and the Author Application Form at www.awsdetroit.org or www.ewi.org. The completed Author Application Form and abstract should be sent to Menachem Kimchi, SMWC Technical Chairman, EWI, 1250 Arthur E. Adams Dr., Columbus, OH 43221, (614) 688-5153, FAX: (614) 688-5001, menachem_kimchi@ewi.org.